Microstructure and Mechanical Properties of Friction Stir Welded Similar and Dissimilar Joints of Al and Mg alloys †

SAAD Ahmed Khodir * and SHIBAYANAGI Toshiya**

Abstract

Similar joints of 2024-T3 Al alloys and dissimilar joints of 2024 Al alloy to 7075 Al alloy and AZ31 Mg alloy were produced by friction stir welding (FSW). Effects of FSW parameters such as welding speed, rotation speed and backing materials on microstructure and mechanical properties of similar 2024-T3 Al alloy joints and dissimilar joints of 2024-T3 Al alloy to 7075-T6 Al alloy and AZ31 Mg alloy aluminum alloy. Scanning electron microscopy, with energy dispersive X-ray spectroscopy (EDS) was carried to analyze the homogeneity of constituents in the stir zone (SZ) of dissimilar joints.

An increase of equiaxed grain size in the SZ with increasing rotation speed was observed for all similar and dissimilar joints. Reduction of grain size in the SZ was obtained for similar 2024 Al alloy joints when using type 2 of backing material at the same welding conditions. For dissimilar joints between 2024 and 7075 Al alloys, at a rotation speed of 400min^{-1} there was no mixing of two alloys in the SZ and a border between them was observed. Increase of rotation speed more to than 400min^{-1} brought about a mixed structure resembling onion rings with periodic change of equiaxed grain size and heterogeneous distribution of alloying elements in the SZ. In the case of dissimilar joints between 2024 Al alloy and AZ31 Mg alloy a laminated structure was formed in the SZ near the boundary between SZ and TMAZ on the advancing side of 2024 Al alloy regardless of the welding speed. Hardness values increased with increasing rotation speed and fluctuated in the SZ of dissimilar joints due to formation of onion rings and intermetallic compounds. In the case of defect-free joints, tensile strength increased with increasing rotation speed and backing plate of type 3 brought about the best tensile properties for similar 2024 Al alloy joints.

KEY WORDS: (2024 Al Alloy) (Dissimilar Joint) (7075-T6 Al Alloy) (AZ31 Mg Alloy) (Friction Stir Welding) (Rotation and Welding Speed) (Backing Materials) (Mechanical Properties)

1. Introduction

Defects such as intermetallic components and porosity occurring in the weld region of similar and dissimilar joints of aerospace aluminum and magnesium alloys have long prohibited the use of fusion welding processes for joining these alloys[1,2]. Friction stir welding (FSW) is a relatively new technique invented at The Welding Institute (UK) in 1991 [3] especially for joining aerospace Al alloys[4-9]. Since that time, FSW has been introduced into a number of commercial welding applications include magnesium[10,11], copper[12], steel[13], titanium[14] alloys and dissimilar metal group welding[15-18]. The greatest importance is the fact that the process occurs in the solid state and, therefore, the formation of brittle solidification products is minimized and grain boundary cracking due to liquation does not occur. Heat input is significantly lower than that in the case of fusion welding processes and temperature during welding is less than the melting point of the base metals[19-20].

In this process a welding tool (consisting of a shoulder and probe assembly) is rotated with high speed and plunged into the joint line between two plates to be butt welded together. The frictional heat generated by the welding tool makes the surrounding material softer and allows the tool to move along the joint line. The softened material starts to flow around probe, resulting in a transferring of material from the leading edge of the tool to the trailing side. This stirring action by the rotating tool yields a heavily deformed region in the material. An FSW joint is known to have four zones such as: (i) intensively deformed zone called the stir zone (SZ), (ii) thermomechanically affected zone (TMAZ), (iii) heat affected zone (HAZ) and unaffected base metal (BM) [3-9].

The aim of the present research is to study the influences of FSW parameters on microstructure and mechanical properties of similar 2024-T3 Al alloy joints and dissimilar joints of 2024-T3 Al alloy to 7075-T6 Al alloy and AZ31 Mg alloy aluminum alloy. The present

† Received on June 22, 2007
* Graduate Student
** Associate Professor

Transactions of JWRI is published by Joining and Welding Research Institute, Osaka University, Ibaraki, Osaka 567-0047, Japan

work focused on the weldability and reliability of friction stir butt joints from the metallurgical point of view.

2. Experimental Procedures

The main base metal used in this study was 2024-T3 Al alloy. The other two base metals used for producing dissimilar joining to 2024 Al alloy were 7075-T6 Al alloy and AZ31 Mg alloy. The thickness of all base metals was 3 mm. The chemical composition and tensile properties of the base metals are listed in **Tables 1** and **2**, respectively. All similar and dissimilar welds were performed using a welding tool made of tool steel (SKD61). The welding tool is composed of 12 mm diameter shoulder and 4 mm diameter threaded probe. The tool axis was tilted by 3 degrees with respect to the vertical axis. Effects of welding parameters such as welding speed, rotation speed and backing materials on microstructures, hardness distributions, and tensile properties of the welded joints were investigated. **Table 3** summarizes all welding conditions for similar and dissimilar joints.

Temperatures were measured during FSW for similar 2024 Al alloy joints by utilizing 0.5 mm diameter K-type thermocouple at four positions, the SZ at the center line, the HAZ at the bottom surface in the advancing side, and at a distance of 10 mm either side of the weld center line. Thermocouples were set at the middle distance of the weld length from the start point of welding. After welding, samples from similar and dissimilar joints were cut out using an electric discharge machine. They were then mounded and ground through grit silicon papers up to grade # 2000. For Al alloys, final polishing was performed using 0.3 μm alumina and colloidal silica suspensions, then cleaned in an ultrasonic cleaner with acetone, and dried. For dissimilar jointing of 2024-T3 Al alloy to AZ31 magnesium alloy, final polishing was performed using 0.25 μm diamond suspension solutions with oil. Microstructures of the cross-sectional area of welded joints were then observed, using an optical microscope (OM).

A scanning electron microscope equipped with an energy dispersive X-ray spectroscope (EDS) was used to analyze the homogeneity of constituents in the SZ of dissimilar joints. Crystallographic data collection by Electron Back-Scattered Pattern (EBSP) for BM and SZ of similar 2024-T3 Al alloy joints was performed in the scanning electron microscope with 0.5 μm step size. The EBSP measurement was conducted using a JEOL-JSM 6400 instrument operated at 20 Kv.

Microhardness measurement for similar and dissimilar joints was carried out along the center line at mid-thickness positions of the cross section which is transverse to the welding direction with an internal spacing of 0.5 mm under the load of 0.98 N for 15 s loading time. To determine the effect of welding parameters of similar and dissimilar joints on tensile properties, tensile test specimens were machined in the transverse directions to the weld line. Tensile tests were carried out at room temperature with a strain rate of 1.2 x 10^{-3} s^{-1}.

3. Results and Discussion

3.1 Microstructures of base metals

Figure 1 shows the microstructures of three base metals. The microstructure of 2024 Al alloy BM is shown in Fig. 1(a), representing elongated grains along the rolling direction with a random distribution of second phase particles revealed as small black particles. These grains of several hundred microns length and approximately 40-70 μm width are lying along the transversal direction that is normal to the welding direction. The microstructure of BM of 7075 Al alloy is shown in Fig. 1(b), representing elongated grains with a slightly different dimension and a lower concentration of second phase particles than that in 2024 Al alloy. The microstructure of BM of AZ31 Mg alloy as shown in Fig. 1(c) is composed of a granular phase of Mg solid solution with remarkable number of deformation twins.

3.2 FSW of similar 2024-T3 Al alloy joints

3.2.1 Microstructures of joint

Figure 2 represents an example of typical microstructures observed in the joint welded at a welding speed of 50 mm/min and a rotation speed of 1250 mm/min. The microstructure of HAZ shown in Fig. 2 (a) is similar to the BM (Fig. 1 (a)) with slightly difference in contrast. Fig.2 (b and e) represents the TMAZ on advancing and retreating sides, respectively, and reveal that the material has been plastically deformed. No recrystallization occurred in this region, and there is generally a distinct boundary between the TMAZ and SZ on the advancing side. On the other hand, the boundary between the TMAZ and SZ is rather unclear on the retreating side of the weld as shown in Fig. 2 (e).

Fig. 2(c) represents the microstructures of SZ where microstructure consisted of equiaxed grains with much smaller size compared to the large elongated grains of BM. Fig.2 (d) represents the microstructure at the bottom surface of the joint. It contains two different microstructures. The first is a fine grain region at the upper side resulted from the action of rotating probe. The second is an elongated microstructure at the lower side remaining from BM. The transition region between HAZ and TMAZ is clearly observed in Fig. 2(f).

3.2.2 Effect of rotation speed on the microstructures of the SZ

Figure 3 shows the recrystallized grain structure with higher magnification at the center position of the SZ for different rotation speeds at a constant welding speed of 50mm/min. Grain size increases with increasing rotation speed. In addition, increasing rotation speed resulted in finer and more homogenous distributions of particles in the SZ. Grain size increases from 2.6 μm at 400 min^{-1} to 7.1 μm at 1000 min^{-1}, while further increase of rotation speed faster than 1000 min^{-1} did not bring about significant increase of grain size. A maximum grain size of 7.8μm was obtained at 1500 $min^{-1}$of the rotation speed.

3.2.3 Effect of welding speed and backing plates on the microstructures of the SZ

Figure 4 shows microstructures of recrystallized grains in the center region of SZ for the joints welded at 50 and 100 mm/min with three types of backing plates.. At 50 mm/min of welding speed, grain size in SZ decreases from 7.4 μm for stainless steel 304 (type 1) backing to 1.7 μm for pure copper block (type 2) while the combination of stainless steel 304 on pure copper block (type 3) resulted in the grain size of 4.4 μm that is between these two types. At 100 mm/min, grain size for backing types 1, 2 and 3 decreases from 7.4, 1.7, and 4.4 to 5.5, 1.3, and 3.6 μm, respectively. Regardless of backing types, grain sizes in the SZ of the joints welded at a higher welding speed were lower than those of the joints welded at lower one due to lower heat input associated with lower welding speeds.

Table 1 Chemical composition of base metals.

Materials	Chemical compositions (mass %)								
	Si	Fe	Cu	Mn	Mg	Cr	Zn	Ti	Al
2024-T3 Al alloy	0.01	0.08	5.35	0.67	2.07	0.09	0.04	0.05	Bal.
7075-T6 Al alloy	0.01	0.08	2.4	0.09	2.52	0.21	7.99	0.06	Bal.
AZ31 Mg alloy	0.01	0.09	0.03	0.43	Bal.	0.01	1.96	0.00	2.83

Table 2 Mechanical properties of base metals.

Materials	Mechanical properties at room temperature		
	Yield stress (MPa)	Tensile stress (MPa)	Elongation (%)
2024-T3 Al alloy	327	461	29.5
7075-T6 Al alloy	498	593	17.7
AZ31 Mg alloy	170	244	16.8

Table 3 Welding conditions.

Joint type	backing plate	Rotation speed (min^{-1})	Welding speed (mm/min)	Fixed location of base metals		Welding tool		
				Advancing side	Retreating side	Shoulder diameter	Probe diameter	Tilt angle
Similar 2024 Al alloy joints	SUS304 (type1)	400	50	2024 Al alloy	2024 Al alloy	12mm	4mm	3 degrees
		600						
		800						
		1000						
		1250						
		1500	50					
			120					
			180					
			250					
	Pure copper (type2)	100	50					
			100					
	Pure copper +0.5mmSUS304 (type 3)		50					
Dissimilar joints between 2024 and 7075 Al alloys	SUS304 (type1)	400	100	2024 Al alloy	7075 Al alloy			
		800						
		1200	40					
			70					
			100					
			200					
		1600	100					
		2000						
Dissimilar joints between 2024 Al alloy and AZ31 Mg alloy		2500	200	2024 Al alloy	AZ31 Mg alloy			
			300					
			400					
			550					

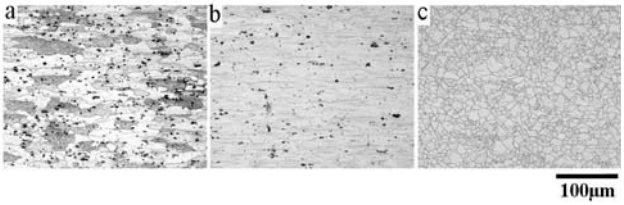

Fig. 1 Microstructures of the base metals (a) 2024 Al alloy, (b) 7075 Al alloy and (c) AZ31 Mg alloy.

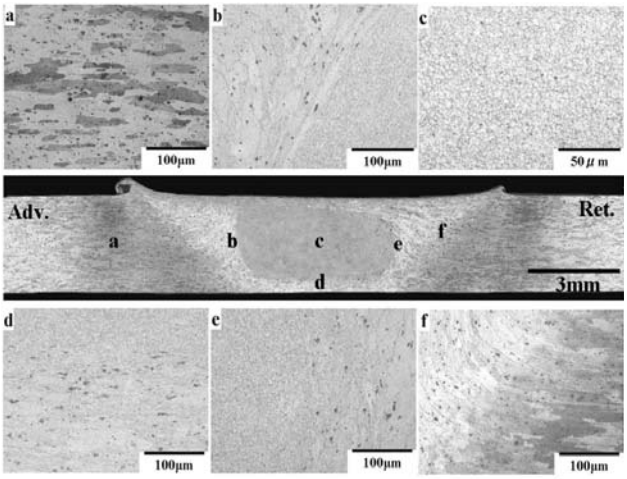

Fig. 2 Microstructures of different regions for the joint welded at 1250 min^{-1} and 50 mm/min.

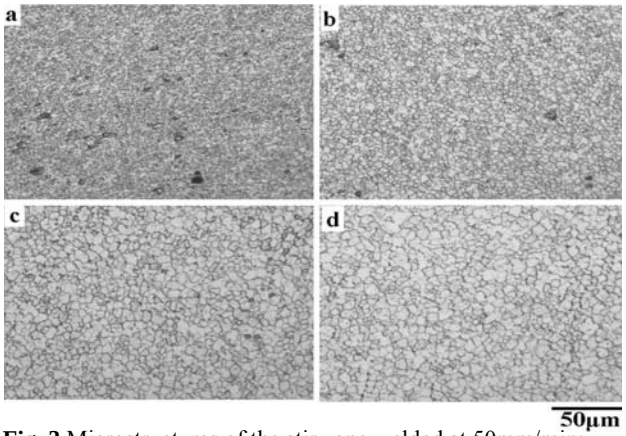

Fig. 3 Microstructures of the stir zone welded at 50mm/min: (a) 400 min^{-1} (b) 600 min^{-1}, (c) 1000 min^{-1}, and (d) 1500 min^{-1}.

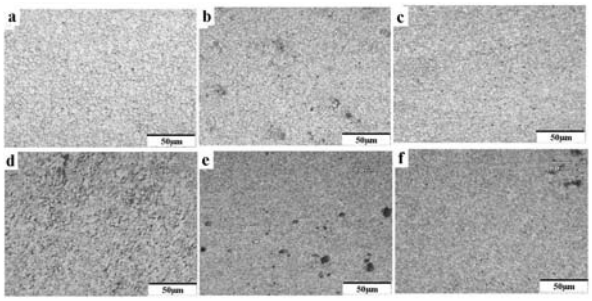

Fig. 4 Microstructures of the SZ: (a type 1, (b) type2, (c) type 3 at 50 mm/min, (d) type 1, (e) type2, (f) type 3 at 1000 mm/min.

3.2.4 Temperature measurements

Table 4 summarizes peak temperatures measured at the bottom center position in the SZ and HAZ for different rotation speeds and three types of backing materials. The peak temperature increases with increasing rotation speed. The increment of temperature in the SZ was 51.5 ^{0}C between 400 min^{-1} and 1000 min^{-1} of rotation speeds, and the incremental was larger than that between 1000 min^{-1} and 1500 min^{-1} (501 ^{0}C at rotation speed 1000 and 523 ^{0}C at 1500 min^{-1}). Temperature in the HAZ increase gradually from 406 ^{0}C at 400 min^{-1} to 438 ^{0}C at 1500 min^{-1} of rotation speed. The joints produced using backing type 2 have the lowest peak temperature of 410 ^{0}C in the SZ and also the lowest value of 398 ^{0}C in the HAZ at 3mm from the welding centerline, while backing type 1 brings about the highest temperatures in both zones; 513 ^{0}C in the SZ and 438 ^{0}C in the HAZ at 6 mm from the weld centerline. For the case of backing type 3 the temperatures were between these two cases. At 100 mm/min of welding speed the temperatures in two the zones decreased for every backing type. A large increment of temperature of 103 ^{0}C is measured in the SZ by changing backing type from 1 to backing type 2. This could be attributed to a considerable amount of heat extraction through the copper block.

Figure 5 shows temperature histories measured at a point in the HAZ during FSW for the backing type 1 (a), type 2 (b), type 3 at a welding speed of 50 mm/min (c), and type 3 (d) at a welding speed of 100 mm/min. In the present study "the welding time" is defined as the entire time starting from 262 ^{0}C to the peak temperature followed by cooling down to this temperature. This temperature range was selected because of the longer time at that temperature range increases the rate of precipitation during over-aging rather than dissolution rate [21]. Peak temperatures are in the order of backing type 1, type 3, type 2 at 50 mm/min and type 3 at 100 mm/min of welding speed indicating the reduction of welding time. The combined effect of Cu-block and higher welding speed results in the fastest welding time as shown in (d).

Heating and cooling rates are defined as T_1 / t_1 and T_1 / t_2 in Fig. 5, respectively in the present study. T_1 is the increment of temperature from 262 ^{0}C to peak value. t_1 and t_2 are times required for reaching peak temperature and time for reaching 262 ^{0}C from peak temperature, respectively. For backing types 1 and 2, heating rates are 17.25 and 25.0 K/s, respectively. Cooling rates for backing types of 1 and 2 were 11.5 and 22.2 ^{0}C/s, respectively. For backing type 3, heating rates were 20.8, and 32.6 ^{0}C/s for welding speeds of 50 and 100 mm/min., respectively. Cooling rates for welding speeds of 50 and 100 mm/min. are 17.0, and 28.12 ^{0}C/s, respectively. Backing type 3 at a welding speed of 100 mm/min has the highest cooling or heating rates while backing type 1 at 50 mm/min has the lowest one.

In general, the average grain size decreases with decreasing working temperature and increasing working stain rate[7]. Since the recrystallized temperature decreases with increasing strain rate or rotation speeds, grain growth proceeds faster as the temperature increases. In the case of backing type 1 the largest grain size is obtained because of the highest peak temperature, as shown in Table 4. Thus the lower grain size in the SZ was brought about by the reduction of peak temperature due to decreasing rotation speed, increasing welding speed or using a higher thermal conductivity backing material such as pure copper. For the backing type 3, the 0.5 mm-thick SUS304 plate added onto the pure copper bock slightly decreased the amount of heat extraction through the copper block which in turn increased the peak temperature resulting in larger grain size. Therefore, grain size in the SZ is expected to be controlled easily by controlling rotation and welding speeds or utilizing suitable backing materials.

3.2.5 Crystallographic data of the BM the and SZ

Figure 6 shows orientation maps and pole figures of the BM and central region in the SZ of a joint welded at 1250 min^{-1} and 100 mm/min using backing type 3. This welding condition was selected for OIM analysis where maximum mechanical properties are achieved as shown later when talking about the hardness and tensile properties of joint. These images in Fig. 6 were constructed such that the misorientation angle was greater than 15^0. The orientations are colored according to the color key of the inverse pole figure (IPF) // WD as shown in the right portion of upper side in Fig. 6. The BM in Fig. 6 (a) shows large grains with high angle grain boundaries. On the other hand, the SZ is composed of equiaxed fine grain structure with a high fraction of high angle grain boundaries as a result of dynamic recrystallization as shown in Fig. 6(b).

A (100) pole figure of the BM indicates that the most dominant component is close to strong rotated cube orientation {001} <110> as shown in Fig. 6(c). The cube texture is well known as a typical recrystallization texture in aluminum alloys. On the other hand, (111) pole figure of the SZ shows that the texture in this region roughly takes the orientations of {114} <221> and {110} <001> as shown in Fig. 6(d). This (111) pole figure was produced by rotation of -16, 10, and 17 degrees about ND, WD and TD, respectively. These two texture components in the central region of the SZ were also observed in 6063-T5 aluminum alloy by Sato *et al*[22]. The change from rotated cube texture of the BM to {114} <221> and {110} <001> textures in the SZ suggest that a complicated metal flow takes place during FSW.

FSW is considered as a shearing deformation process. Shearing and compressive stresses are generated at the surface between the rotating shoulder and the metal surface during rotation and forward motion of tool shoulder. Also shear stresses arise along the probe surface and during its forward motion. The effect of the shoulder is limited to the surface region while the effect of the probe extends from the area under the shoulder to the center area of the SZ[22,23]. The (111) plane is located almost parallel to the axial direction of the rotating probe. Therefore the weak shearing texture <111>// ND in the middle region of the SZ resulted from the shearing stresses arising from the probe surface and its forward motion.

3.2.6 Effect of welding conditions on the hardness distributions of joints

Figure 7 shows microhardness profiles after 4 months of natural aging. The measurements were performed across the SZ, TMAZ, HAZ, and BM on a transverses cross-section of joints welded at a constant welding speed of 50 mm/min and different rotation speeds. Increasing rotation speed has a large influence on the hardness of the SZ and TMAZ but slightly effective for the HAZ. The SZ and TMAZ hardened with increasing rotation speed and the hardness values almost reached that of the BM at a rotation speed of 1000 min^{-1}. This could be attributed to the increase of temperature which may be sufficient to force larger precipitates to be dissolved and reprecipitate again in the weld during natural aging.

Soft zones existed on both sides of the HAZ where some precipitates might have coarsened and lost their coherency due to the thermal history. The hardness value in the HAZ slightly increases as rotation speed rises. Although increasing rotation speed resulted in larger grain size in the SZ (Fig. 3), hardness increased as rotation speed increased regardless of the coarsening of grains in the SZ. This tendency suggests that significant increase of hardness with increasing rotation speed is not a function of grain size but a function of the size and distribution of second phase particles and precipitates. Grain size is less effective for hardening behavior in the SZ compared with other factors.

Figures 8 and **9** show profiles of microhardness distributions for the joints welded at a welding speed of 50 and 100 mm/min, respectively using backing plates of type 1(a), type 2(b) and type 3(c). Hardness changed greatly in the SZ and HAZ depending on backing materials. The position of hardness minimum shifted from 6 mm for type 1 to 3 mm for type 2 from the weld center and the value increased and reached a maximum among the present joints in case of the backing type 3 and at a welding speed of 100 mm/min. This change of hardness distribution clearly suggests that selection of backing plate is quite important for controlling mechanical properties of FSW joints as well as microstructure. In case of backing type 1 as shown in Fig. 9(a) comparing with Fig.8 (a), no significant hardness change appears in the SZ both at lower and higher welding speeds. On the other hand, the HAZ becomes harder and higher welding speed brings about further hardening of the HAZ and a maximum value of about 110 Hv at 6.0 mm from the weld center line is achieved, while the value is still much lower than that of the BM. For backing types 2 and 3, as shown in Fig. 9(b)

and (c), respectively, the HAZ shows further increase of hardness and the maximum value increases by 14-16Hv over that welded at lower welding speed when compared with Fig. 8(b) and (c). The difference of hardness values in the HAZ between types 2 and 3 is about 2-3 Hv, while larger differences of about 14-16 Hv are obtained between backing type 1 and types 2 or 3. On the contrary, the SZ for backing type 3 becomes harder than type 2.

Table 4 Temperature measured in the SZ and HAZ.

Welding speed (mm/min)	Rotation speed (min^{-1})	Type of backing plate	SZ Temperature/ ^{0}C	HAZ Temperature/ ^{0}C
50	400	1	450	406
	1000		501	-
	1250		513	438 (at 6mm from WCL)
	1500		523	-
50	1250	2	410	398, 262 (at 3, 6mm from WCL)
50		3	471	418 (at 3mm from WCL)
100			435	375 (at 3mm from WCL)

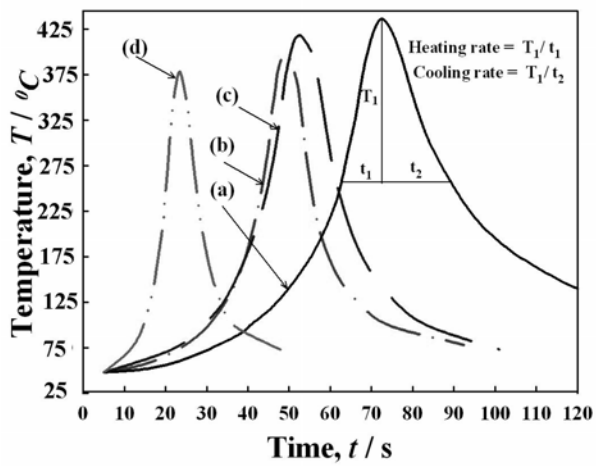

Fig. 5 Temperature change with time at the HAZ during FSW for different backing materials: (a) type 1, (b) type 2, (c) type 3 at 50 mm/min and (d) type 3 at 100 mm/min of welding speed.

In general higher welding speed results in higher hardness since less frictional heat is introduced into the materials and the present data is consistent with this general rule. The results shown in Figs. 8 and 9 suggest that improvement of hardness distribution is realized not only by higher welding speed but also by selecting the type of backing materials. In 2024-T3 Al alloy BM, the initial hardening agent is Guinier Preston Bagarystskii (GPB) zones[24]. These zones dissolve during heating resulting in very fine S' or S precipitates (Al_2CuMg) without slight changes in hardness. Upon continuous heating to higher temperatures S' or S precipitates coarsen and lose their coherency[24,25]. Softening behavior observed in the HAZ could be caused by a coarsening and/or a dissolution of S' or S precipitates during welding. Hardening in the SZ could be attributed to the formation of new GPB zones at room temperature after welding[25].

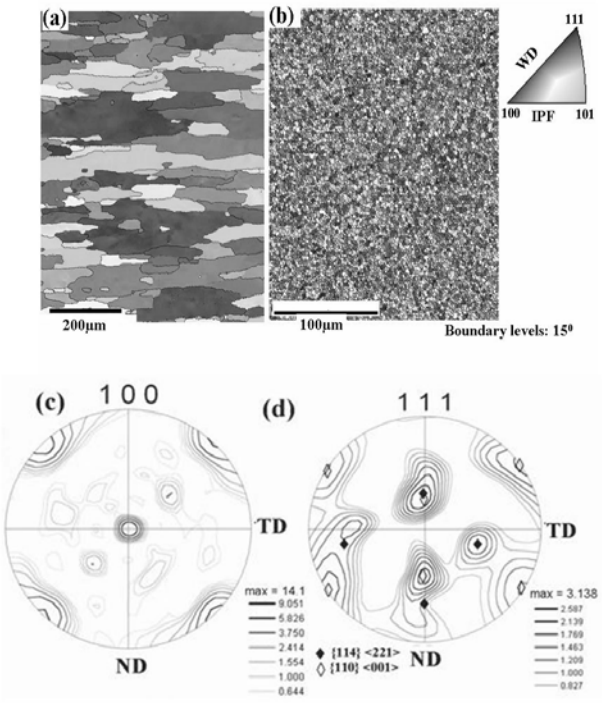

Fig. 6 Orientation maps and pole figures of the BM and SZ: (a) orientation map of the BM, (b) orientation map of the SZ, (c) 100pole figure of BM, (d) 111 pole figure of the SZ.

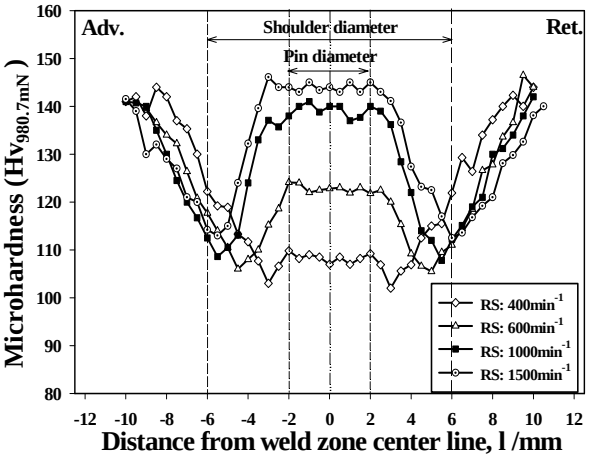

Fig. 7 Hardness profiles at mid thickness transverse to welding directions for different rotation speeds.

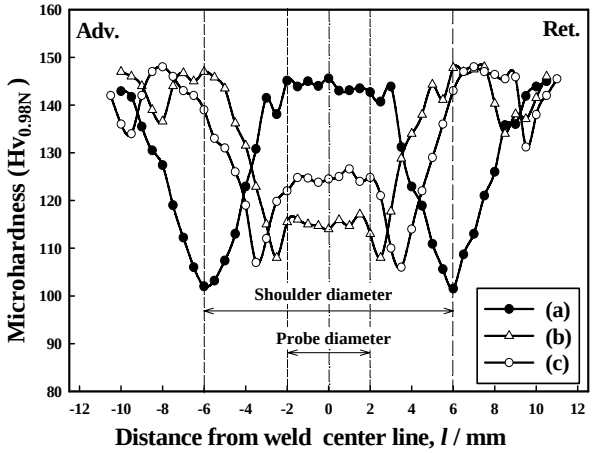

Fig. 8 Hardness profiles at mid thickness transverse to welding directions of the weld joint for: (a) backing type 1, (b) type 2, and (c) type 3.

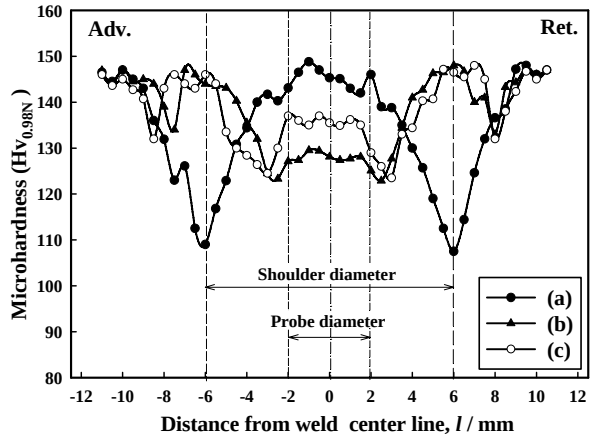

Fig. 9 Hardness profiles at 100mm/min welding speed: (a) for backing type 1 (b) type 2, and (c) type 3.

The best condition achieving hardness distribution close to the ideal state in similar 2024-T3 Al alloy joints is obtained by utilizing the backing plate of type 3 together with a welding speed of 100 mm/min., although the distribution still showed a hardness drop in the SZ. But additional natural aging or artificial aging treatments are expected to be effective for reducing the fluctuation of hardness. Also, designing backing materials having appropriate thermal conductivity and heat capacity would be promising for obtaining small fluctuations of hardness throughout the friction stir welded joints.

3.2.7 Tensile properties of joints

Table 5 shows the tensile properties of joints welded with different rotation speeds, welding speeds and backing materials. In case of backing type 1, tensile strength, yield strength, and elongation increased with increasing rotation speeds and decreasing welding speed. The lowest tensile properties were obtained for the joint welded at 400 min^{-1} due to lower hardness and presence of severe kissing bonds at the root of weld. Also, due to kissing bonds and small segments observed at the top surface for joints welded at 1500 min^{-1} and different welding speeds, the tensile properties of joints slightly decreased less than those of joint welded at 1250 min^{-1}.

At 50 mm/min of welding speed and 1250 min^{-1} of rotation speed, tensile strength, yield strength, and elongation of backing type 2 are lower than those for backing type1 although larger minimum values of hardness are obtained in case of backing type 2. This could be attributed to a kissing bond at the welding root of the joint. The maximum tensile strength and elongation to fracture of the joints are 427 MPa and 14.3%, respectively, which are achieved at 100 mm/min of welding speed and using backing type 3, where higher hardness is obtained.

When joints are free from defects, their tensile properties are only affected by the microhardness distributions[26]. As seen in Fig. 7, increasing tensile strength of joints could be attributed to a slight increase of hardness in the HAZ. Also, when the joints are free from defects, the joints are fractured on the retreating side instead of the advancing side. Temperature measurements at 10 mm from both sides of welding center line at 800 min^{-1} of rotation speed were 311 ^{0}C on the retreating side and 304 ^{0}C on the advancing side. Higher temperature resulted in softening on the retreating side and hence fracture occurred on this side. This result indicates that the tensile strength on the advancing side is higher than that on the other side. The advancing side shows slightly higher hardness than the other side.

Although the hardness distributions with higher value is achieved in the cases of backing types 2 and 3, the tensile properties of joints in the case of type2 are much inferior to those of type3. The lower tensile properties of joints using type 2 could be attributed to the lower temperature on the bottom surface of welded joints which should affected the metal flow in this area especially at higher welding speed, where kissing bond appeared. The addition of a 0.5 mm SUS304 plate on the Cu-block keeps temperature relatively high at the bottom surfaces which made joints free from kissing bonds.

Table 5 Mechanical properties and fracture locations of welded joints.

Type of backing plate	Rotation speed (min^{-1})	Welding speed (mm/min)	Fracture locations	Tensile properties of welded joints		
				Yield stress (MPa)	tensile stress (MPa)	Elongation (%)
1	400	50	SZ	253.7	335	5.5
	600		HAZ of Ret. side	275	378.5	8.5
	800		HAZ of Ret. side	285.7	386.8	9.5
	1000		HAZ of Ret. side	291	394.5	11.3
	1250		HAZ of Ret. side	294	402	12.4
	1500	50	Border between SZ and TMAZ	290	376	8
		120	SZ	235	373	7.5
		180		260	351	5
		250		242	321	4.2
2	1250	50		272	340	8.0
		100		276	374	6.0
3		50	HAZ of Ret. side	275	385	11.0
		100	HAZ of Ret. side	284	427	14.3

3.3 FSW of dissimilar 2024-T3 to 7075 –T6 Al alloys

3.3.1 Effect of rotation speed

Figure 10 shows the macroscopic appearance of the cross-sections of the dissimilar joints produced at different rotation speeds. In case of 400 min^{-1} a border appears between the two alloys indicating that no mixing of alloys occurred in the weld zone as shown in Fig. 10(a). The grey and brighter zones corresponded to 2024 and 7075 Al alloys, respectively. In cases of 800, 1200, and 1600 min^{-1} of the rotation speeds, as shown in (b), (c), and (d) of Fig. 10, onion ring patterns were clearly observed in the SZ. The onion ring was more clearly visible on the advancing side than retreating side. These bands are clearly visible on the advancing side than retreating side, which usually appears not only in dissimilar aluminum alloys friction stir welded joints but also in similar ones. At a rotation speed of 2000 min^{-1} the SZ decreases its area and becomes irregular shape with unclear onion ring. The size of the SZ increased with increasing rotation speed till 1200 min^{-1} of rotation speed due to increasing strain and heat input. However, larger rotation speed above 1200 min^{-1} resulted in decreasing area of the SZ. This could be attributed to the excess amount of metal removed from the weld zone at higher rotation speeds. All joints welded at different rotation speeds are free from other defects such as porosity and tunnel like defects.

Figure 11 shows grain structures for different rotation speeds in the center region of the SZ. Average grain size increases with increasing rotation speed with a periodic change of grain size which is clearly observed in Fig. 11(c). The average grain sizes of smaller and larger grains are 4.2 μm and 5.7 μm, respectively. The grain size increases with increasing rotation speed due to increasing heat input[3,7]. Average grain size increases from 3.1 μm at 400 min^{-1} to 5.9 μm at 2000 min^{-1}. The effect of welding speed on the average grain size in the SZ was similar to that for similar joints of 2024 Al alloy where the average grain size in the SZ decreased with increasing welding speed.

3.3.2 EDS analysis of joints

Figure 12 shows a result of SEM-EDS analysis performed at the center position of the SZ for a joint welded at 400 min^{-1}. A clear border between two regions having clearly different contrasts is observed by a back-scattered electron image (BEI) as shown in Fig. 12(a). The corresponding X-ray images of Cu-Kα and Zn-Kα are shown in (b) and (c), respectively. Cu and Zn are the main alloying elements in 2024 and 7075 Al alloys, respectively. As shown in (b), Cu is enriched in the left side region suggesting that this region is occupied by the 2024-T3 Al alloy. The other area on the right side of border is abundant in Zn as seen in (c) indicating that this region is occupied by 7075-T6 Al alloy.

Quantitative EDS line analysis of Cu and Zn was then carried out along the center line in the SZ, transverse to the welding direction and the result is shown in Fig. 12(d). The content of Cu fluctuated from 5.1 to 6.3 mass% in the left side region of the border and decreased to 1.8-2.9 % just after crossing the border to the retreating side. On the other hand, the composition of Zn increased sharply upon crossing the border from 0.2 % on the advancing side to about 5.7-8.5 % on the other side. The composition on the left side related to the 2024 Al alloy while that at the right related to 7075 Al alloy. These differences in chemical composition observed on both sides of border suggest that there was no chemical mixing occurring between the two materials in the SZ in case of lowest heat input.

Figure 13 shows results of SEM-EDS analysis near the

advancing side of the SZ, for a joint welded at 100 mm/min of welding speed where 2024 Al alloy was fixed on the advancing side. The bands of onion ring are clearly visible in the middle part of the BEI image as shown in Fig. 13(a). The X-ray images of Cu, Zn, and Mg, are shown in (b), (c), and (d), receptively. The brighter bands in Fig. 13(a) were abundant in Zn while the darker bands were rich with Cu and Mg. Therefore, the darker bands observed in Fig. 13(a) is related to the 2024 Al alloy while the brighter ones are related to the 7075 Al alloy.

Table 6 summarizes the results of EDS quantitative analysis for Cu, Zn, Mg and Mn at the positions indicated in Fig. 13(a). The concentrations of Cu and Mn in the positions 1, 3, and 5 were almost corresponding to their contents in the 2024 Al alloy while the concentrations of Zn and Mn at the positions 2, 4 and 6 were close to the 7075-T6 Al alloy. The Mg content at the locations 1, 3 and 5 was slightly higher than its content in the 2024 Al alloy and was lower than that in the 7075 Al alloy at locations 2, 4 and 6. This may be related to the diffusion of Mg inside the SZ.

From the results mentioned above, it should be emphasized that the heterogeneous distribution of alloying elements in the SZ was achieved. This heterogeneity in microstructures through the SZ could be attributed to the insufficient welding time required for completing diffusion of alloying elements in the SZ. Also, it should be concluded that the onion ring pattern reflects the difference in chemical composition as well as grain size between the lamellar bands in the nugget.

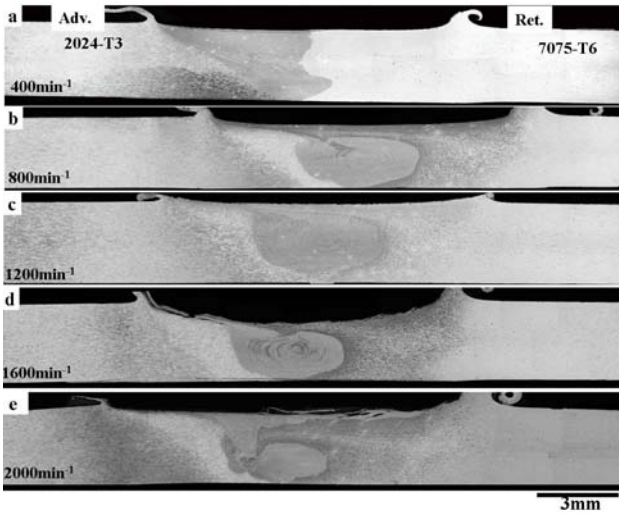

Fig. 10 Macrostructures of joints welded at different rotation speeds: (a) 400, (b) 800, (c): 1200, (d) 1600, and (e) 2000 min^{-1}.

3.3.3 Hardness of joints

Figure 14 shows Vickers microhardness profiles of joints welded at different rotation speeds after 3.5 Ms (forty days) of natural aging. The SZ shows a great change of the hardness distribution with increasing rotation speed. The minimum hardness value in the HAZ of the 2024 Al alloy located at about -4.0 mm from the center while the HAZ of the 7075 Al alloy had a minimum hardness value at about 7.5mm from the center. This may be attributed to the difference of precipitation behavior between the two alloys under a given thermal history during the joining. The abrupt increase of hardness just beyond the center towards the retreating side in the joint welded at 400 $min^{-1}$is caused by the change of materials from 2024 to 7075 Al alloy, where no mixed structure was obtained as shown in Fig. 12(a).

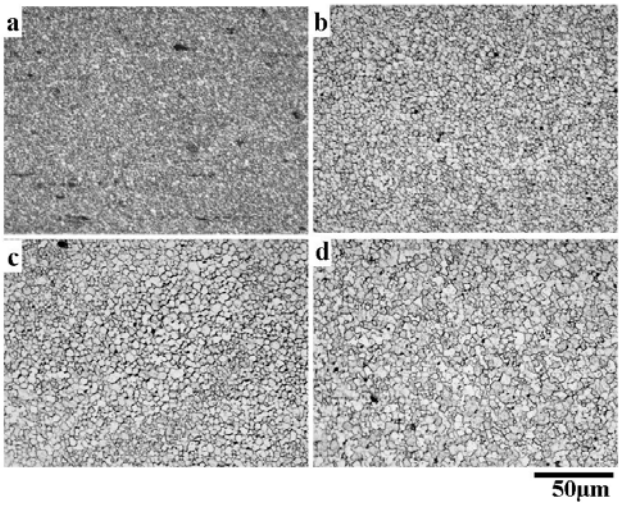

Fig. 11 Microstructures of the SZ of the joints where AA2024-T3 fixed at advancing side: (a) 400 min^{-1}, (b) 800 min^{-1}, (c) 1600 min^{-1} and (d) 2000 min^{-1}.

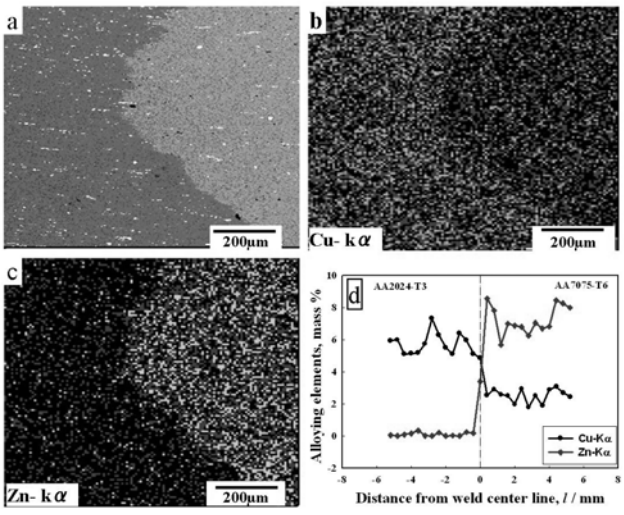

Fig. 12 SEM and EDS analysis of the SZ of a joint welded at 400 $min^{-1}$of rotation speed: (a) SEM image of boundary line in the center of the SZ, (b) EDS image of Cu, (c) EDS image of Zn, (d) EDS line analysis of Cu and Zn.

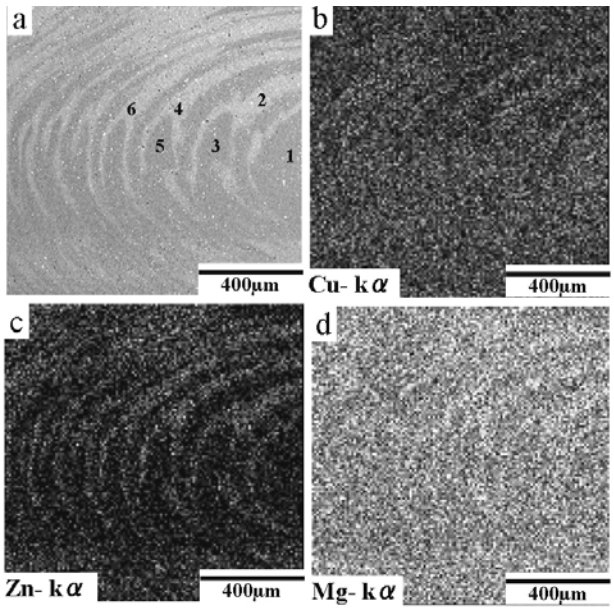

Fig. 13 SEM and EDS images of the SZ of the joint welded at 100mm/min of welding speed: (a) SEM image of the SZ, (b) EDS image of Cu, (c) EDS image of Zn, and (d) EDS image of Mg.

Table 6 EDS quantitative analysis of zones corresponding to Fig. 13(a).

Alloying elements	Content / mass%					
	1	2	3	4	5	6
Cu	5.9	2.6	5.80	2.7	5.7	2.4
Zn	0.2	7.7	1.06	7.4	0.4	6.8
Mg	2.7	1.3	2.82	1.4	1.3	1.3
Mn	0.8	0.2	0.5	0.2	0.6	0.1

In case of the rotation speed of 1200 min^{-1}, hardness increased and fluctuated from 143 to 150 Hv in the SZ due to the formation of onion ring patterns where bands of a periodic alteration of composition from 2024 and 7075 Al alloys are observed. Increasing rotation speed has a significant influence on the hardness distribution of the SZ but is less effective for the HAZs in the two alloys. Also, increasing rotation speed has a significant influence on the TMAZ of 2024 Al alloy side but slightly effective on that of the other side.

Softened zones exist on both sides of the HAZs of the two materials. In these zones some precipitates might have coarsened and lost their coherency due to the thermal history. But the minimum values on the 7075 Al alloy side are higher than that those on the 2024 Al alloy side. This could be attributed to the higher hardness value of 7075 Al alloy BM (163 Hv) than that of the 2024 Al alloy (145 Hv). Both HAZs of the two alloys slightly harden as the rotation speed rises. At 2000 min^{-1} the hardness in the SZ is slightly decreased but the distribution is more homogenous than that at 1200 min^{-1}.

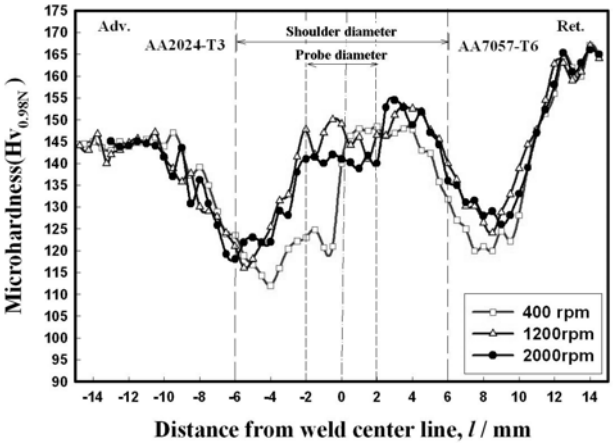

Fig. 14 Hardness profiles at mid thickness transfers to the welding directions of the welded joints for different rotation speeds where AA2024 fixed on the advancing side.

3.3.4 Tensile properties of joints

Table 7 summarizes the tensile properties and fracture locations measured for dissimilar joints welded at different welding and rotation speeds. Tensile strength increased with increasing welding and rotation speeds up to 100 mm/min and 1200 min^{-1}, respectively, but still lower than those of two base metals. Elongation of the joints is much lower than that of the 2024-T3 BM but slightly lower than the 7075-T6 BM. Its maximum value was about 14.9 % at 100 mm/min and 1200 min^{-1} when the 2024 Al alloy was fixed on the advancing side. The maximum tensile strength of the joints was 423 MPa which was achieved at 1200 min^{-1} of rotation speed and 100 mm/min of welding speed when the 2024 Al alloy was fixed on the advancing side.

The lowest tensile strength was obtained for the joint welded at 2000 min^{-1} due to the presence of cracks in the top surface region as shown in Fig. 10(e). Fracture occurred in the HAZ on the 2024 Al alloy side for all the defect-free joints whereas the SZ becomes the region of fracture for the joints including defects such as kissing bonds at the root or cracks at the top surface. The hardness distribution of the joint welded at 400 min^{-1} reveals that the weakest region is located in the HAZ on the advancing side as shown in **Fig. 14**. Therefore the fracture occurred in this region instead of the border between the non-mixed alloys regions appearing in the SZ.

3.4 FSW of dissimilar join 2024 alloy to AZ31 Mg alloy

3.4.1 Effect of welding speed

Figure 15 shows macroscopic appearances of the

cross-section of the dissimilar joints produced at different welding speeds. Kissing bond was only the defect observed in the bottom region for all welding speeds. The SZ consists of three regions with different contrast such as grey, dark grey and bright. As shown in Fig. 15(a), (b) the bright region tended to exist mainly in the SZ on the retreating side, while middle portion of the SZ near the advancing side is occupied by grey or dark grey regions. Increasing welding speed to more than 300 mm/min changed the location of bright contrast region structure to the lower portion of the SZ near the bottom surface as shown in Fig. 15(c) and (d). Also, increasing welding speed to more than 300 mm/min brought about the change in location of the grey and dark grey regions to the upper portion of the SZ beneath the tool shoulder as shown in (c) and (d). The bright and dark grey regions corresponded to the 2024-T3 Al alloy and the AZ31 Mg alloy, respectively while grey region corresponding to a mixture of them.

The position changes of these structures in SZ may be attributed to the alternation of metal flow that depends on the welding speed. Since Mg alloys have inferior formability to Al alloys, increasing welding speed or decreasing heat input makes Mg alloy related regions less mobile around the probe, and eventually the region comes to concentrate in the hotter region which locates under the tool shoulder. A lamellar-like band where either the 2024 Al alloy related region or the AZ31 Mg alloy is lying one on another. This laminated structure is observed in the SZ near the boundary between the SZ and TMAZ of 2024 Al alloy on the advancing side.

Table 7 Mechanical properties and location of fracture of welded joints in the transverse direction to the weld center line.

Welding speed (mm/min)	Rotation speed (min-1)	Tensile properties			
		AA2024-T3 located in advancing side			
		Yield strength (MPa)	Tensile strength (MPa)	Elongation (%)	Fracture location
100	400	291.0	399.0	14.0	HAZ of 2024
	800	286.0	407	14.3	HAZ of 2024
40	1200	274.8	395.0	13.6	HAZ of 2024
70		281.5	404	15.5	HAZ of 2024
100		290	423	14.9	HAZ of 2024
200		287	398	11.4	SZ
100	1600	283	392	12.5	SZ
	2000	273.5	363	7.5	SZ

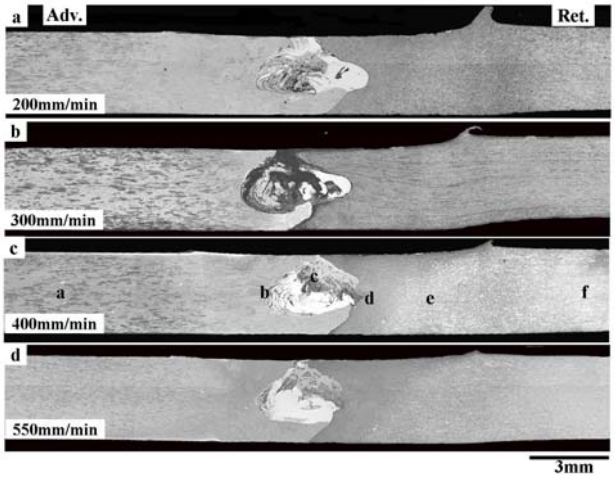

Fig. 15 Macrostructures of joints welded at different welding speeds: (a) 200, (b) 300, (c): 400 and (d) 550 mm/min.

Figure 16 shows an example of typical microstructures observed in the joint welded at a welding speed of 400 mm/min. Figure 16(a) represents a microstructure of the TMAZ and laminated bands in the SZ on the advancing side of a 2024 Al alloy. The grain size in the TMAZ is almost the same as that in the BM and grains were bent by about 45 degrees indicating the severe plastic deformation in this region. Fig. 16(b) shows a microstructure of the SZ where grey and slightly dark grey regions are observed. The grey region consists of grains with irregular shape. This region includes some small fragments probably coming from the Mg alloy side where fine grain structure is represented in the right part of Fig. 16(b). The slightly dark grey region in the left part of Fig. 16(b) consists of equiaxed grains with much smaller size compared to those in the BMs on both sides. The size of recrystallized grains in this area ranges from 3 to 6.7 μm, and these grains belong to the AZ31 Mg alloy.

Figure 16(c) represents the microstructure of the TMAZ on the AZ31 Mg alloy side in the joint. No deformation structure such as twins and elongated grains was observed. The grains are also equiaxed and recrystallized having a size equal to that in the SZ. This result is consistent with the report by N. Afrin[27] on similar FSW of Mg alloy. These features in microstructure are considered to be

different from the cases of other similar FSW of Mg alloys[10,11] as well as most of the Al alloys where the TMAZ was characterized by bent and elongated grains as in the TMAZ of 2024 Al alloy side in the present study. The microstructure of the HAZ is shown in (d) and is similar to the microstructure of the BM of AZ31 Mg alloy. Grain sizes in the SZ and TMAZ of the Mg alloy side decrease with increasing welding speed due to decreasing heat input. The average grain size decreases from 8.2 μm at 200 mm/min to 4.4 μm at 550 mm/min.

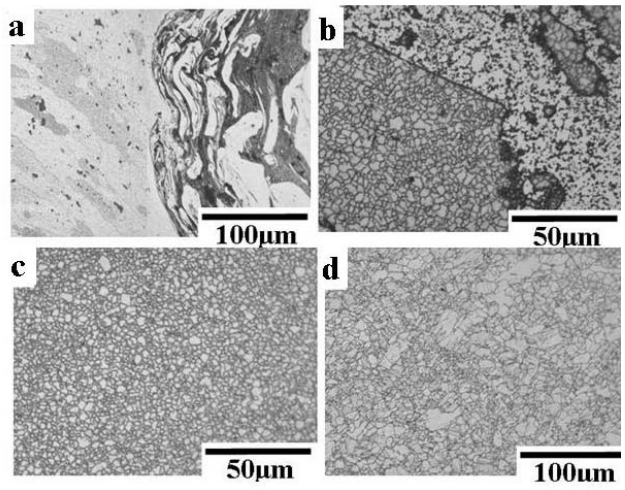

Fig. 16 Microstructures at different location of joint corresponding to Fig.15(c).

3.4.2 EDS analysis of joints

Figure 17 shows a result of SEM-EDS analysis for the joint welded at 550 mm/min. Three regions such as grey, slightly dark grey and dark grey having clearly different contrasts are observed by back-scattered electron image (BEI) as shown in Fig. 17(a). The slightly dark grey and dark grey regions are concentrated in the upper region of the SZ. The corresponding X-ray images of Al-Kα and Mg-Kα are shown in (b) and (c), respectively. As shown in Fig. 17(b), Al is enriched in the lower region of the SZ suggesting that this region is occupied by the 2024 Al alloy. The brighter region in Fig. 17(c) at upper region of the SZ was abundant in Mg while the darker ones were mainly rich with Mg. This result indicates that the region in the upper region of the SZ is occupied by AZ31 Mg alloy.

Table 8 summarizes the results of EDS quantitative analysis for the regions corresponding to Fig. 17(a). The mass percentages of Mg and Al at the positions 1, 3, 6, 9, and 10 were almost corresponding to the intermetallic compounds of Al_2Mg_3 or $Al_{12}Mg_{17}$ [28] observed in the SZ. These positions are located in the microstructure having irregular shape which is shown in the upper region of Fig. 16(a). The positions 2, 8 and 11 were almost corresponding to 2024 Al alloy which is represented in brighter regions of Fig. 15. The concentrations of Mg and Zn at the positions 4, 5, 7 and 12 were close to those of AZ31 Mg alloy.

The effect of welding speed on the microstructure of weld joints is a heterogeneous distribution of elements in SZ which is similar to that in dissimilar joints between 2024 and 7075 Al alloys. In addition, the results of SEM-EDS analysis clearly suggest that a localized region in SZ experienced constitutional liquation or melting during FSW which upon cooling solidifies to produce the intermetallic compound in the SZ. This is consistent with the previous studies[28,29] on FSW of dissimilar joints between other Al alloys and AZ31 Mg alloy. The temperature in the SZ for all welding speeds might be higher than the melting points of eutectic reaction (460 ^{0}C) occurring between Al and Mg in the binary phase diagram.

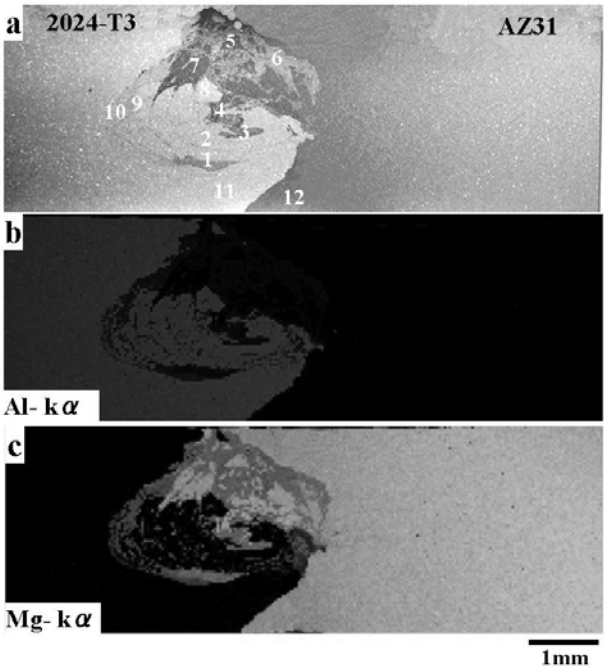

Fig. 17 SEM and EDS images of joint welded at 550 mm/min of welding speed: (a) SEM image of weld joint, (b) EDS image of Al and (c) EDS image of Mg.

3.4.3 Effect of welding speed on hardness of joints

Figure 18 shows microhardness profiles of joints welded at 200, 400 and 550 mm/min. The measurement was carried out across the nugget on the transversal cross-section normal to the welding directions. The BMs of 2024 Al and AZ31 Mg alloys have average hardness values of 143 and 60 Hv, respectively. The hardness value in the SZ varies from 65 to 220 Hv due to the presence of intermetallic compounds as well as Al and Mg phases. The lower hardness value of 65Hv corresponds to the AZ31 region while the higher values from 140 to 220 Hv are caused by the intermetallic phases. No significant change in hardness distributions was observed in the SZ between 200, 400 and 550 mm/min of welding speed.

On the other hand, increasing welding speed has a significant influence on the hardness distribution in the HAZ and TMAZ of the 2024 Al alloy side but is less

effective for the AZ31 Mg alloy side. This is directly related to the fact that the 2024-T3 Al alloy is an age hardening alloy which is affected by the thermal history during welding, while the AZ31 Mg alloy is a solid solution. The slight increase in hardness by about 5 Hv in the regions in the SZ occupied by Mg alloy and the TMAZ on the AZ31 Mg alloy side could be attributed to the grain refinement in these regions. On the contrary, hardness in the BM increases with decreasing grain size according to the Hall Petch equation.

Table 8 EDS quantitative analysis of zones corresponding to Fig. 17(a).

Alloying elements	Content / mass%											
	1	2	3	4	5	6	7	8	9	10	11	12
Al	30.84	92.2	37.02	8.63	2.68	34.53	2.79	84.27	39.45	58.1	90.65	2.42
Mg	63	1.56	59.01	88.89	94.35	60.09	94.33	10.23	58.51	36.35	1.77	94.56
Cu	3.07	5.18	2.34	0.69	0.14	2.69	0.04	4.6	0.97	2.98	5.98	0.08
Zn	2.05	0.41	0.81	1.22	2.26	1.65	2.30	0.03	0.77	1.26	0.34	1.93
Mn	0.63	0.59	0.63	0.32	0.41	0.62	0.28	0.78	0.24	0.8	0.73	0.65

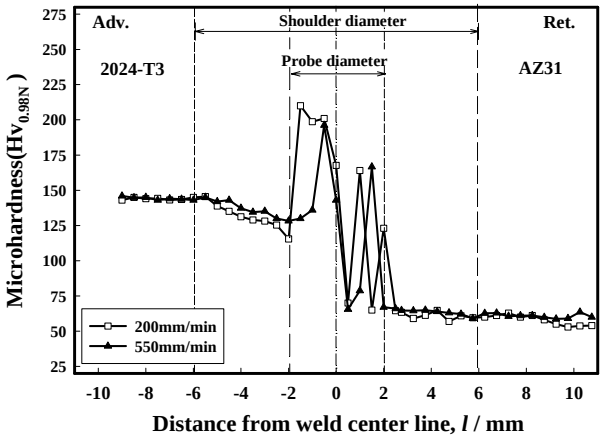

Fig. 18 Hardness distributions for the joints welded at 200 and 550mm/min of welding speed

Conclusions

(1) An increase of equiaxed grain size in the SZ with increasing rotation speed was observed up to 1000 min^{-1} of rotation speed. Increasing rotation speed faster than 1000 min^{-1} did not bring about significant increase of grain size in the SZ. Reduction of grain size in the SZ was achieved when using type 2 backing material at the same welding conditions. Larger grain size in the SZ was obtained using backing type.

(2) Hardness increased in the SZ and TMAZ as the rotation speed increased. Also, increasing welding speed brought about significant improvement in hardness in the HAZ with slight change in the SZ at a constant rotation speed of 1500 min^{-1}.

(3) Hardness changed greatly in the SZ and HAZ depending on backing materials. The position of hardness minimum shifted from 6 to 3 mm from the weld center and the value increased and reached a maximum among the present joints in case of the backing type 3 and at a welding speed of 100mm/min.

(4) Backing plate of type 3 brought about the best tensile properties.

(5) In the case of dissimilar joints between 2024 and 7075 Al alloys, at the rotation speed of 400 min^{-1} there was no mixing of the two alloys in the SZ and a border was observed between them irrespective of the fixed location of materials. Increase of rotation speed at any welding speed brought about a mixed structure and an onion ring pattern was formed with a periodic change of equiaxed grain size and heterogeneous distribution of alloying elements in the SZ. At 2000$min^{-1}$of rotation speed and 100 mm/min of welding speed, the onion ring pattern disappeared and the composition of the SZ mainly consisted of the 2024 Al alloy.

(6) At 400 min^{-1} of rotation speed of dissimilar joints between 2024 and 7075 Al alloys, higher hardness was obtained in the SZ of the 7075 Al alloy side in the joint where no mixing took place between two alloys. At higher rotation speed than 400 min^{-1} and all ranges of welding speed, hardness increased with increasing rotation speed and fluctuated in the SZ due to the formation of onion ring patterns. Hardness minimum was in the HAZ on the 2024 Al alloy side and its values increased with increasing welding speed. Also hardness in the HAZ slightly increased with increasing rotation speed.

(7) In the case of tensile tests, the defect-free joints were fractured in the HAZ on the 2024-T3 Al alloy side of the dissimilar joints between 2024 and 7075 Al alloy while the defect-containing joints fractured in the SZ. Maximum tensile strength of the joints of 423 MPa was achieved at 1200 min^{-1} and 100 mm/min.

(8) In the case of dissimilar joints between 2024 Al alloy and AZ31 Mg alloy, increasing welding speed led to redistribution of phases in the SZ where the regions occupied by 2024Al alloy concentrated in the lower

part of the SZ, while AZ31 Mg alloy concentrated in the upper regions just beneath the tool shoulder. A laminated structure was formed in the SZ near the boundary between the SZ and TMAZ on the advancing side of 2024 Al alloy regardless of welding speed.

(9) The SZ of dissimilar joints between 2024 Al alloy and AZ31 Mg alloy consists of three main regions occupied by the microstructure of the 2024 Al alloy, AZ31 Mg alloy, and irregular structure containing of some fragments from the Mg Alloy.

(10) The irregular-shaped regions and laminated structure in the SZ of dissimilar joints between 2024 Al alloy and AZ31 Mg alloy contained large volume of intermetallic compounds which were formed by constitutional liquation during welding. The hardness distribution in the SZ is slightly affected by welding speed and the harness values varied from 65 to 220 Hv due to the presence of intermetallic compounds and microstructures occupied by either 2024 Al alloy or AZ31 Mg alloy.

Acknowledgements

This work was supported by a grant-in-aid for scientific research B (project No. 17360353) and a grant-in-aid for cooperative research project of nationwide joint-use Research Institutes on Development Base of Joining Technology for new Metallic Glasses and Inorganic Materials from The Ministry of Education, Science, Sports and Culture, Japan.

References

1) C.J. Dawes and W.M. Thomas: Weld. J. Vol. 75 (1996), p 41- 45.
2) M. B. Kannan, W. Dietzel, R. Zeng, R. Zettler and J.F. Santos: Mater. Sci. Eng. In press (2007).
3) R. S. Mishra and Z. Y. Ma: Mater. Sci. Eng. R Vol. 50 (2005), p1-78.
4) C. G. Rhodes, M. W. Mahoney, W. H. Bingel, R. A. Spurling and C. C. Bampton: Scripta Materialia, 36 (1997) 69-75.
5) O. V. Flores, C. Kennedy, L. E. Murr, D. Brown, S. Pappu, Brook M. N. and J. C. McClure: Scripta Materialia 38 (1998) 703-708
6) J.-Q. Su, T. W. Nelson, R. Mishra and M. Mahoney: Acta Materialia 51 (2003) 713-729.
7) S. Benavides, Y. Li, L. E. Murr, D. Brown and J. C. McClure: Scripta Materialia 41 (1999) 809-815.
8) M. A. Sutton, B. Yang , A. P. Reynolds and J. Yan: Mater. Sci. Eng. A 364 (2004) 66-74.
9) M. A. Sutton, B. Yang , A. P. Reynolds and R. Taylor: Mater. Sci. Eng. A 323 (2002)160-166.
10) J. A. Esparza, W. C. Davis, E. A. Trillo and L. E. Murr: J. Mater. Sci. Lett. 21 (2002) 917-920.
11) W. Xunhong and W. Kuaishe: Mater. Sci. Eng. A 431 (2006) 114-117.
12) H. S Park, T. Kimura, T. Murakamic, Y. Naganod, K. Nakata c and M. Ushio: Mater. Sci. Eng. A 371 (2004) 160-169.
13) A. P. Reynolds, W. Tang, T. Gnaupel-Herold and H. Prask: Scripta Materialia 48 (2003) 1289-1294.
14) W. Lee, C. Y. Lee, W. S. Chang, Y. M. Yeon, S. B. Jung: Mater. Letters 59 (2005) 3315- 3318.
15) J. Ouyang, E. Yarrapareddy and R. Kovacevic: J. Mater. Process. Technol. 172 (2006) 110-122.
16) H. Uzun, C. D. Donne, A. Argagnotto, T. Ghidini and C. Gambaro: Materials & Design 26 (2005) 41-46
17) J. Yan, Z. Xu, Z. Li, L. Li and S. Yang: Scripta Materialia 53 (2005) 585-589.
18) A. C. Somasekharan and L. E. Murr: Mater. Characterization 52 (2004) 49-64.
19) K. V. Jata and S. L. Semiatin: Scripta Materialia 43 (2000) 743-749.
20) C. I. Chang, C. J. Lee and J. C. Huang: Scripta Materialia 51 (2004) 509-514.
21) H. R. Shercliff, J. R. Michael, A. Taylor and T. L. Dickerson: Mecanique & Industries 5 (2005) p 25-35.
22) Y. S. Sato, H. Kokawa, K. Ikeda, M. Enomoto, S.Jogan and T. Hashimoto: Metall. Mater. Trans A 32 (2001)941-948.
23) D. P. Field, T. W. Nelson, Y. Hovanski and K. V. Jata: Metall. Mater. Trans A 32 (2001)2869-2877.
24) C. Genevois, A. Deschamps, A. Denquin and B. Doisneau-cottignies: Acta Mater. 53(2005)2447-2458.
25) M. J. Jones, P. Heurtier, C. Desrayaud, F. Montheillet, D. Allehaux and J.H. Driver: Scripta Materialia 52 (2005) 693-697.
26) H. J. Liu, H. Fujii, M. Maeda and K. Nogi: J. Mater. Process. Technol. (2003) 692-696.
27) N. Afrin, D. L. Chen, X. Cao and M. Jahazi: Mater. Sci. Eng. A (2007), Article in press.
28) Y. S. Sato, C. H. Seung, M. Michiuchi and H. Kokawa: Scripta Materialia 50 (2004) 1233-1236.
29) R. Zettle: Advanced Eng. Mater. 8 (2006) 415-421.